Asymmetric q-Gaussian functions to fit the Raman LO mode band in Silicon Carbide

Amelia Carolina Sparavigna

Department of Applied Science and Technology, Polytechnic University of Turin, Italy

Email: amelia.sparavigna@polito.it

Torino, September24, 2023.

Abstract

Previous studies (Sparavigna, 2023) have demonstrated the Tsallis q-Gaussian functions suitable for the analysis of Raman spectra. Here we consider two asymmetric forms of them, with the aim of further improving the fitting of Raman spectra. The first asymmetric form, that we are here proposing for the first time, is a generalization of the Breit-Wigner-Fano function. The other profile is that made by two different half q-Gaussian functions, chosen to fit the two sides of a Raman band. The case study that we will discuss in detail is that of the Raman LO mode of Silicon Carbide.

Keywords: Tsallis q-Gaussian distribution, asymmetric q-Gaussian distribution, Breit-Wigner-Fano distribution, Raman spectroscopy.

q-Gaussian functions, also known as "Tsallis functions", are probability distributions derived from the Tsallis statistics (Tsallis, 1988, 1995, Hanel et al., 2009). The q-Gaussians are based on a generalized form of the exponential function (see discussion in Sparavigna, 2022), characterized by a continuous parameter q in the range $1 < q < 3$. As given by Umarov et al., 2008, the q-Gaussian function is based on function $f(x) = Ce_q(-\beta x^2)$, where $e_q(.)$ is the q-exponential function and C a constant. In the exponent, we use $\beta = 1/(2\sigma^2)$, with variance σ. The q-exponential has expression: $exp_q(u) = [1 + (1 - q)u]^{1/(1-q)}$, which possesses a bell-shaped profile. In the case that we have the peak of the function at position x_o, the q-Gaussian is given as:

q-Gaussian $= Cexp_q(-\beta(x - x_o)^2) = C[1 - (1 - q)\beta(x - x_o)^2]^{1/(1-q)}$

For q equal to 2, the q-Gaussian is the Cauchy-Lorentzian distribution (Naudts, 2009). For q close to 1, we have the usual Gaussian form. For the q-parameter between 1 and 2, the shape of the q-Gaussian function is intermediate between the Gaussian and the Lorentzian profile. This behavior turns the q-Gaussian into a function suitable for the analysis of Raman spectra, where the spectral bands are characterized, in the same manner, by intermediate profiles between Lorentzian and Gaussian outlines (Kirillov, 2004a). Besides these two functions, which remain the most popular for fitting Raman spectra, *linear combinations* (pseudo-Voigt distributions) or *convolutions* of them (Voigt distributions) are used too (Meier, 2005). The Voigtian function is essentially a Lorentzian height weighted by a Gaussian profile.

Gaussian, Lorentzian, Voigtian and pseudo-Voigtian functions, such as the q-Gaussians are symmetric functions. In fitting the Raman bands, we have encountered peaks which are asymmetric. For instance, in the case of Diamond, (see SSRN), we had the necessity to use three q-Gaussians to fit the asymmetric

Raman peak of the synthetic diamond spectrum. Of course, the presence of more bands producing what looks like an asymmetric peak can be motivated by physical reasons; in any case, alternative approaches can be used to fit asymmetric profiles, for instance by means of Breit-Wigner-Fano (BWF) functions or by pseudo-Voigt (Schmid et al., 2014) or Voigt asymmetric profiles (Ciuryło et al., 1993).

For what is regarding the BWF functions, which are based on Lorentzian functions, we are here proposing their q-generalized form, that is a form based on the q-Gaussian exponential (to the best of author knowledge, this is the first time a q-BWF function is proposed). However, to substitute the asymmetric pseudo-Voigtian or Voigtian functions, a different form of asymmetric q-Gaussian function exists, and it is that used by S. Devi, 2021, for modeling the financial market dynamics. The asymmetric q-Gaussian is made by two different half q-Gaussians, chosen to fit the two sides of the band.

Here we consider q-BWF functions and asymmetric q-Gaussians in some cases. A specific discussion will be devoted to the Raman LO mode band of Silicon Carbide. Let us start form the q-BWF function.

q-BWF function

The Breit-Wigner-Fano function is given as:

$$BWF = C\frac{\left[1 + \xi\gamma^{1/2}(x - x_o)\right]^2}{[1 + \gamma(x - x_o)^2]}$$

In it, ξ is the asymmetry parameter (see Hasdeo et al., 2014, for the use of Breit-Wigner-Fano line shapes for the Raman spectrum of graphene). Parameter γ is the reciprocal of the width. We could generalize the BWF in the q-form (q-BFW):

$$\text{q-BWF} = C\left[1 + \xi\beta^{1/2}(q - 1)^{1/2}(x - x_o)\right]^2 [1 + (q - 1)\beta(x - x_o)^2]^{1/(1-q)}$$

However, we can further generalize the asymmetric form in the following manner:

$$\text{q-BWF} = C\left[1 + \xi\beta^{1/2}(q - 1)^{1/2}(x - x_o)\right]^{2\alpha} [1 + (q - 1)\beta(x - x_o)^2]^{1/(1-q)}$$

When q=2, α=1, we have the function BWF.

Hasdeo and coworkers are giving, in their Eq.(1), the BWF line shape composed by three terms: "a constant continuum spectrum, a discrete Lorentzian spectrum, and an interference effect between both spectra". The interference term is producing the asymmetry of the profile, according to the positive and negative values of argument (x-x_o). The dimensionless ξ parameter is "mimicking the ratio between the probability amplitude of the continuum spectra to that of the discrete spectra" (Hasdeo et al., 2014).

In Prawer and Nemanich, 2004, we can find mentioned the asymmetry of Raman peaks according to some specific effects; we find also the "phonon confinement effects for finite crystal domains" (Richter et al., 1981). In Campbell and Fauchet, 1986, we can easily see the effects of microcrystal size on the shape of Raman spectra. In their Fig.4, an asymmetric peak for a thin film of silicon on saphire (SOS) is shown.

2

Let us start from fitting with q-BWF the curve proposed in the Fig.3(a) by Hasdeo et al. (data have been recovered from the figure). The continuous curve is given by Hasdeo and coworkers according to a theoretical model. The fitting result is shown in the following Figure 1. We can see that the q-BWF is a BWF function, as expected by the theory.
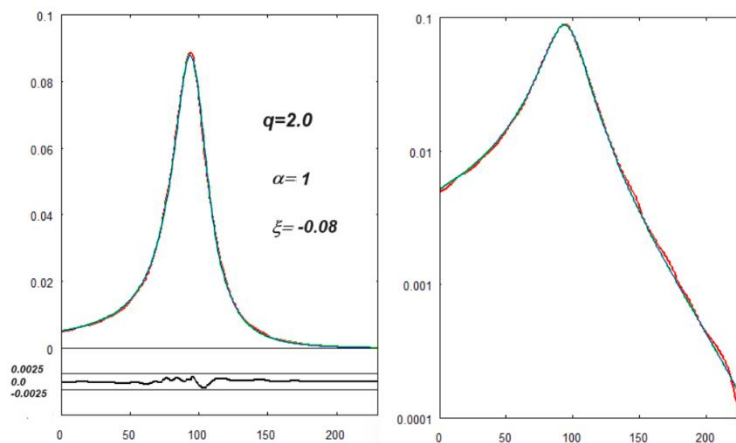

Fig. 1: The best fit (blue) onto the curve (red) given by Hasdeo et al. A q-BWF is used (the values of α, ξ and q-parameters are given in the figure). The misfit is proposed in the lower part of the plot. On the right, the same fit is shown with the log scale for y-axis (semi log scale). Data and q-BWF are given as functions of integers n (equally spaced points), for the x-axis which is representing the Raman shift. A convenient scale is used for the y-axis (intensity axis). The fitting calculation is obtained by minimizing the sum of the squares of the deviations (sum from n=1 to n=660). The value of this sum is 5.5 x 10^{-5}. Some misfit exists but it is due to the recovering of data from the figure in Hasdeo et al.

Let us consider the work by Campbell and Fauchet, 1986, and their Fig.4, with the peak at 524.5 cm^{-1} for a thin film of silicon on sapphire (SOS).
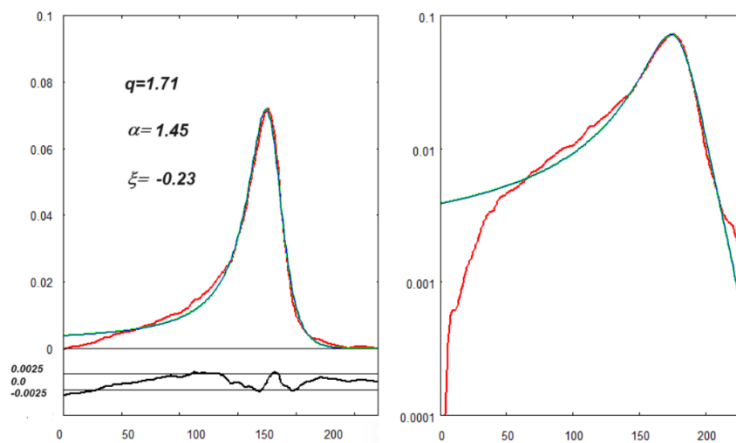

Fig. 2: The best fit (blue) onto the curve (red) given by Campbell and Fauchet, 1986. A q-BWF is used (the values of α, ξ and q-parameters are given in the figure). The misfit is proposed in the lower part of the plot. The fitting calculation is obtained by minimizing the sum of the squares of the deviations (sum from n=1 to n=230). The value of this sum is 8.5 x 10^{-4}.

3

Then, let us try to apply the q-BWF to a specific case, that of the Raman LO mode band of a material which possesses remarkable properties, such as a high thermal conductivity (Sparavigna, 2002), that is, the Silicon Carbide. Data are obtained from the Raman Open Database, a database developed in the framework of the project SOLSA H2020 (El Mendili et al., 2019). In the file at the web page https://solsa.crystallography.net/rod/1000172.html , it is told that the Raman spectrum is related to a 6H-SiC structure, sampled from a terrestrial moissanite, locality at 150 km NW from Izmir, Turkey. About the moissanite and the LO mode in SiC see please Chafai et al., 2001, Rashid et al., 2016, Koyanagi et al., 2016, Liu et al., 2010, Xu et al., 2008, Kiefert et al., 2002, and Shiryaev et al., 2011.
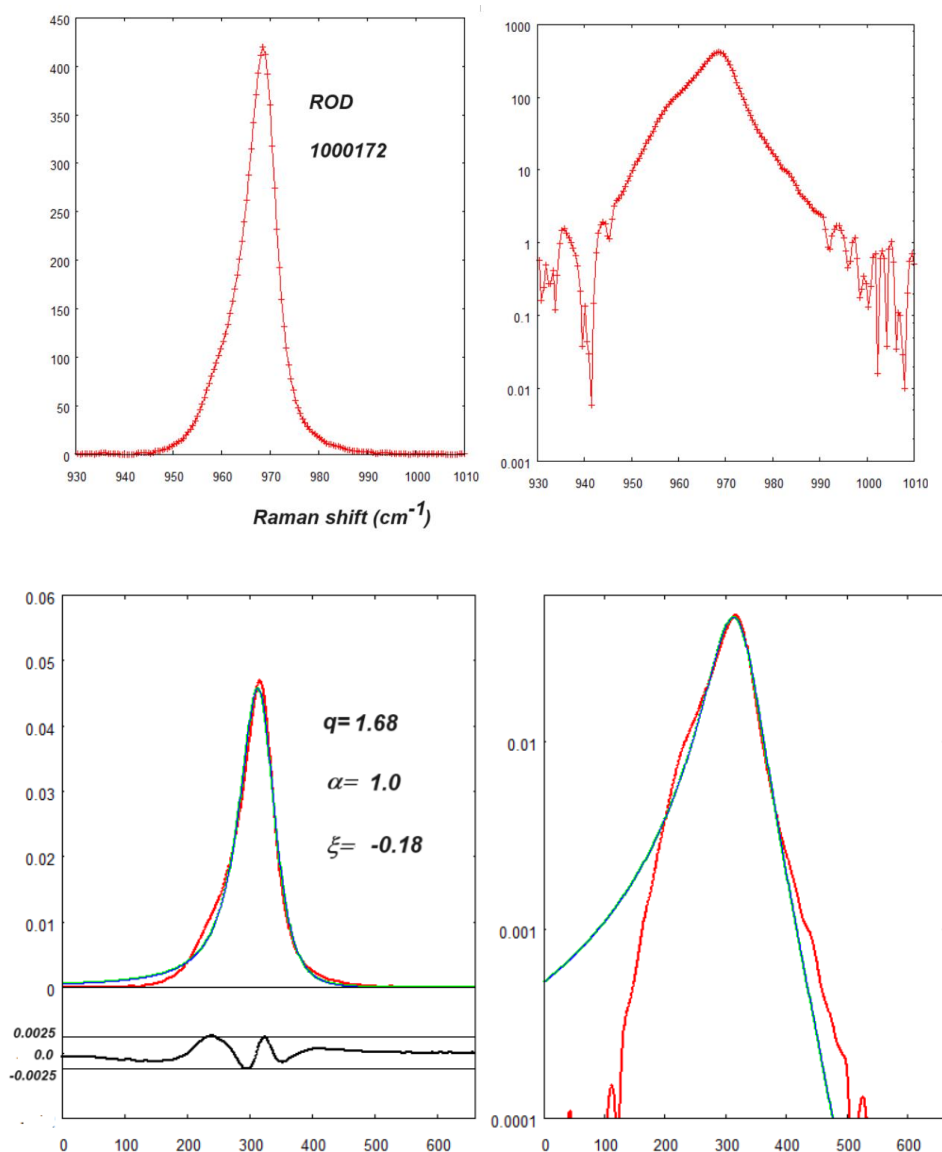

Fig.3: Upper part: data of ROD 1000172 (related ref. Capitani et al., 2007) of the LO mode band (peak at position 968.5 cm^{-1}). On the right, the data with log scale y-axis (semi log scale). Lower part: the best fit (blue) onto data (in red). A q-BWF is used (the values of parameters are given in the figure). The fitting calculation is obtained by minimizing the sum of the squares of the deviations (sum from n=1 to n=660). The value of this sum is 6.6 x 10^{-4}.

4

The fit is rather good. However, it seems that the peak at 968.5 cm^{-1} has a left shoulder; moreover, the left wing is not properly fitting the data, as we can easily see in the semi log scale. So let us consider fitting this peak with the other form of the asymmetric q-Gaussians, but before we must consider the fitting with the symmetric q-Gaussians.

Symmetric q-Gaussians for LO mode SiC

In the following plots, the fits by means of symmetric q-Gaussians are shown for the same LO mode in SiC, which we have previously considered.
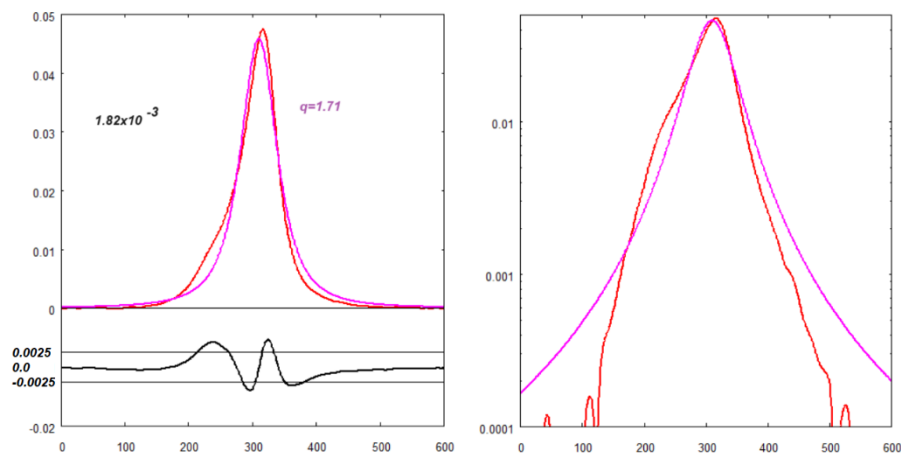

Fig.4: The best fit (magenta) onto data (red) of ROD 1000172 (related ref. Capitani et al., 2007). A symmetric q-Gaussian is used. The sum of the squares of the deviations (sum from n=1 to n=660) is equal to 1.82 x 10^{-3}.
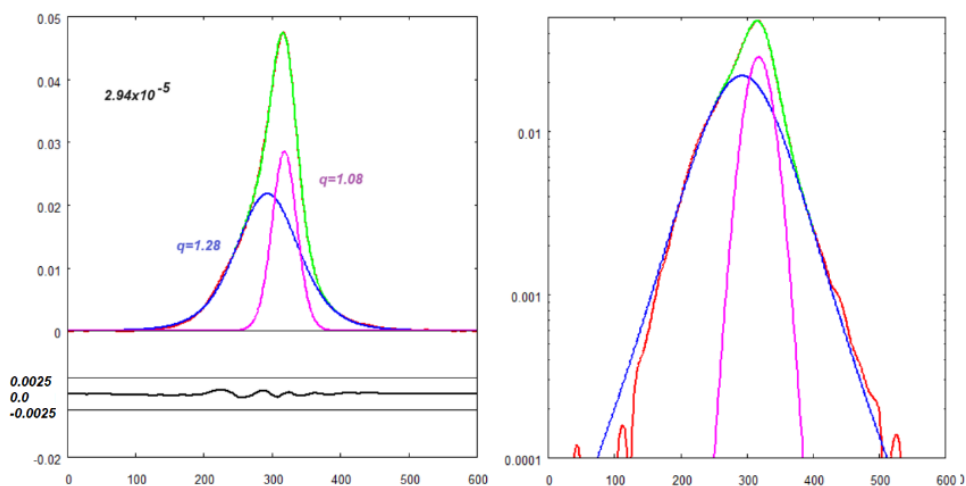

Fig.5: The best fit (green) onto data (red) of ROD 1000172 (related ref. Capitani et al., 2007). Two symmetric q-Gaussians are used (magenta, blue). The sum of the squares of the deviations (sum from n=1 to n=660) is equal to 2.94 x 10^{-5}.

5

In the Figure 5 we have a good fit, however the result is posing a question. We have two components with the same approximate height: are these components adequate to describe the peak, or further components are required? Let us add a third component on the left (Fig.6), and then a further component on the right (Fig.7).
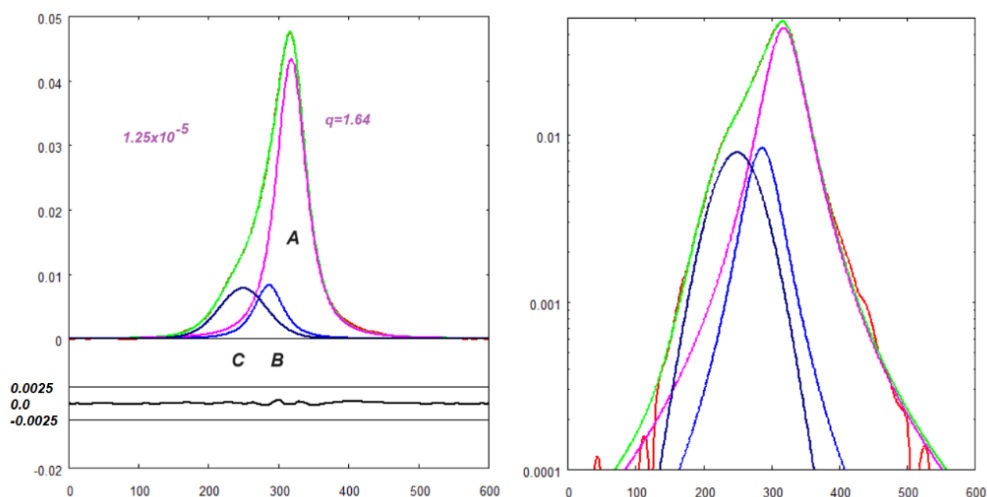

Fig.6: The best fit (green) onto data (red) of ROD 1000172 (related ref. Capitani et al., 2007). Three symmetric q-Gaussian have been used (A, B and C). The sum of the squares of the deviations (sum from $n=1$ to $n=660$) is equal to 1.25×10^{-5}.
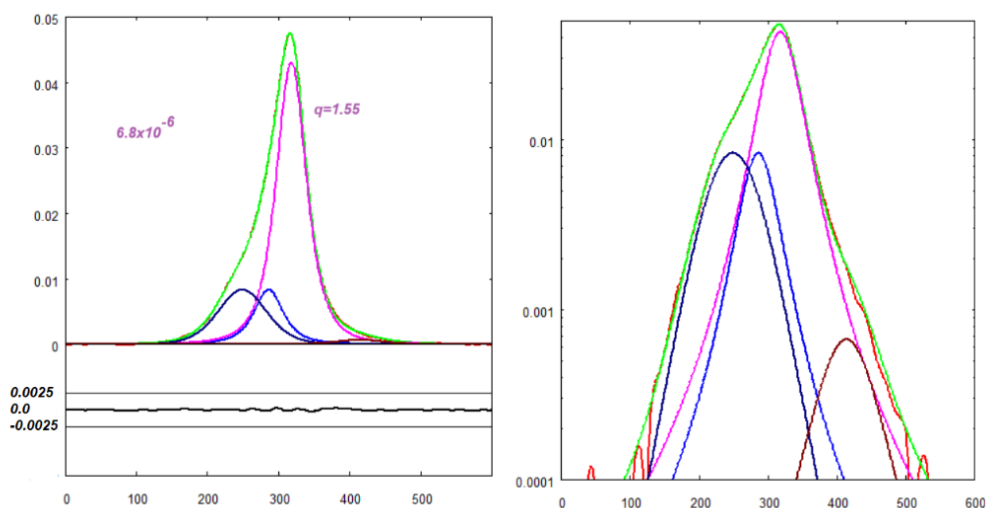

Fig.7: The best fit (green) onto data (red) of ROD 1000172 (related ref. Capitani et al., 2007). Four symmetric q-Gaussian have been used. The sum of the squares of the deviations (sum from $n=1$ to $n=660$) is equal to 6.8×10^{-6}.

6

Asymmetric Tsallis q-Gaussian lines

Figures 6 and 7 are evidencing that, if we use a fitting model based on symmetric q-Gaussians, we can have a main component and a relevant shoulder on its left. This suggests us that we can try to fit the peak in the three following asymmetric manners. The first is that of using a single asymmetric function. The second manner is to imagine A and B components (see Fig.6) merged in an asymmetric function and the C component represented by a symmetric q-Gaussian. The third manner is that of fitting A with a symmetric q-Gaussian and B and C merged into an asymmetric function. Instead of using the previously proposed q-BWF function (Fig.4), here we consider the asymmetric Tsallis q-Gaussians as given in Devi, 2021, that is:

q-Gaussian$_{\text{LEFT}} = Cexp_{q_L}(-\beta_L(x-x_o)^2) = C[1-(1-q_L)\beta_L(x-x_o)^2]^{1/(1-q_L)}$,

when $x - x_o < 0$

q-Gaussian$_{\text{RIGHT}} = Cexp_{q_R}(-\beta_R(x-x_o)^2) = C[1-(1-q_R)\beta_R(x-x_o)^2]^{1/(1-q_R)}$,

when $x - x_o > 0$

Parameters q and β of the two half parts are different.

Here in the resulting plots with one and two components. The Fig.8 is the peak fitted in the first manner, with a single asymmetric q-Gaussian.
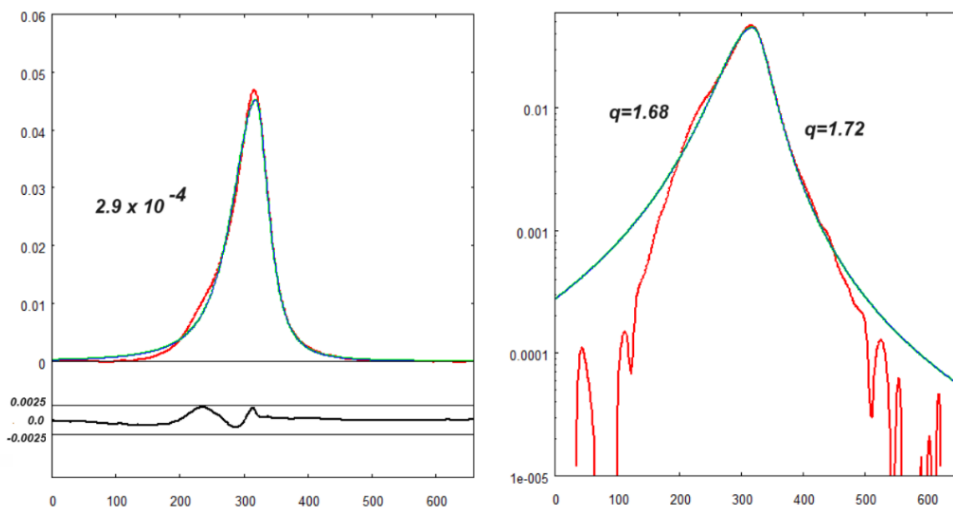

Fig.8: The best fit (blue) onto data (red) of ROD 1000172 (related ref. Capitani et al., 2007). An asymmetric q-Gaussian has been used. The sum of the squares of the deviations (sum from n=1 to n=660) is equal to 2.9 x 10^{-4}.

7

Fig.9: The best fit (green) onto data (red) of ROD 1000172 (related ref. Capitani et al., 2007). An asymmetric (blue) q-Gaussian and a q-Gaussian (magenta) have been used. The sum of the squares of the deviations (sum from n=1 to n=660) is equal to 1.55 x 10^{-5}.

The second manner is that of a fit with a main asymmetric component and a shoulder on the left (Fig.9). We could also add a further component to the right of the band, but this is not increasing information about the role of asymmetry.

A discussion about the use of one or two mode methods for the asymmetric LO band was proposed by Sun et al., 2013. Their Fig.4 is suggesting us the use of the third method of fitting, that is the use of a symmetric q-Gaussian function for the largest component and an asymmetric q-Gaussian for the should om its left.
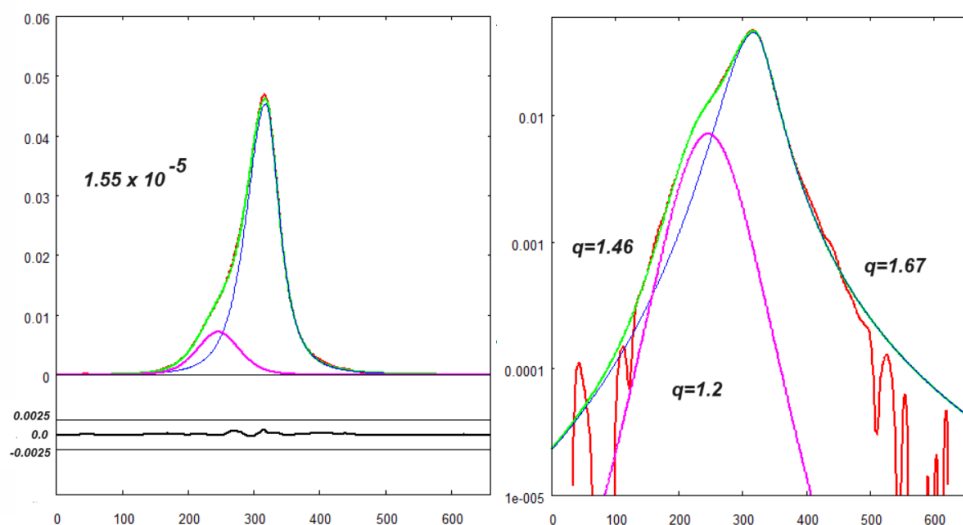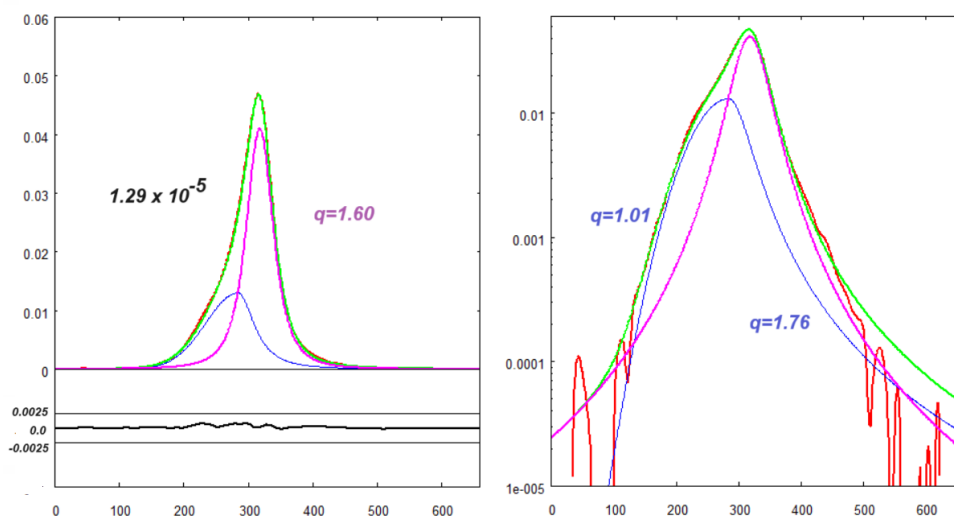

Fig.10: The best fit (green) onto data (red) of ROD 1000172 (related ref. Capitani et al., 2007). An asymmetric (blue) q-Gaussian and a q-Gaussian (magenta) have been used. The sum of the squares of the deviations (sum from n=1 to n=660) is equal to 1.55 x 10^{-5}.

8

The results proposed in the previous plots, regarding the case of the LO mode of SiC are encouraging for applying the asymmetric q-Gaussian to fit the bands of the Raman spectrum.

Let us conclude adding the fit with asymmetric q-Gaussians of the data by Campbell and Fauchet, 1986, which seems being good too.
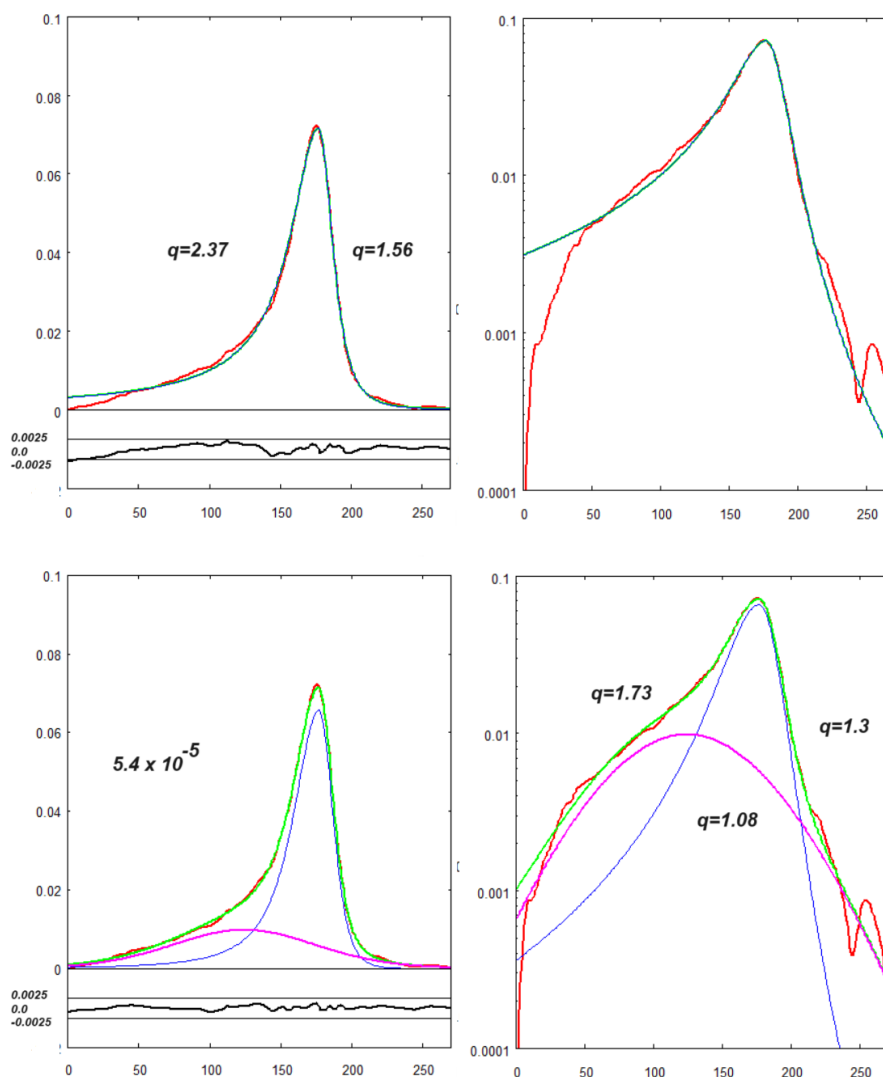

Fig. 11: The best fit (blue) onto the curve (red) given by Campbell and Fauchet, 1986. Upper part: an asymmetric q-Gaussian is used (the values of the q-parameters are given in the figure, note that one of them is larger than 2). The misfit is proposed in the lower part of the plot. The fitting calculation is obtained by minimizing the sum of the squares of the deviations (sum from n=1 to n=260). The value of this sum is 3.5 x 10^{-4}. The fit seems being slightly better than that proposed in the Fig. 2. Lower part: an asymmetric q-Gaussian and a q-Gaussian are used for the fit. Parameters q are given in the panel on the right. The sum of the squares of deviations is equal to 5.4 x 10^{-5}.

9

The fit in the lower part of the Fig.11 is showing the case with an asymmetric main component and a flat q-Gaussian shoulder. If we use an asymmetric shoulder and a symmetric main component (see Fig.12), the result turns out being worse 1.4×10^{-4}. Note that the asymmetric function in the Fig.12 is like that shown in the Fig.10.
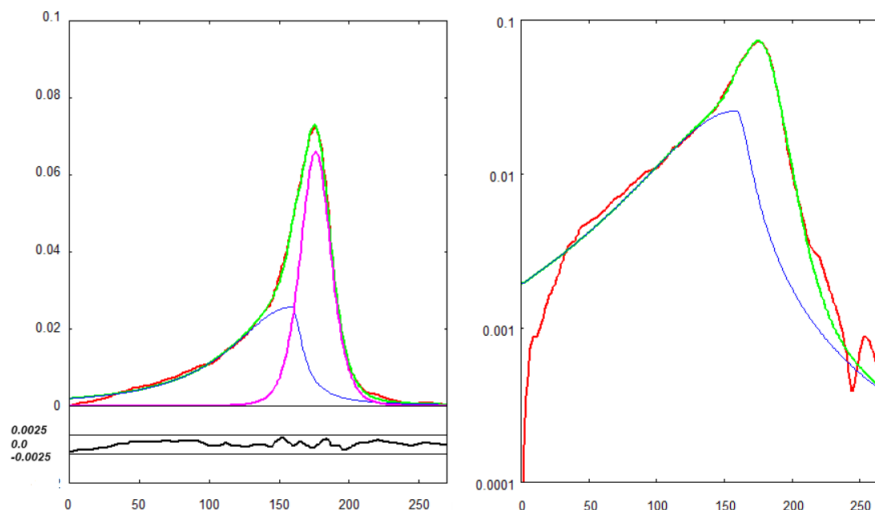

Fig. 12: Using an asymmetric shoulder and a symmetric main component, the result turns out being worse than that given in the Fig.11 (lower part).

Discussion about asymmetry

For our discussion we start from the work by Wieligor et al., 2005, which is displaying the Raman spectra of silicon carbide in the form of small particles and nanowires. It is observed that SiC has the main Raman peaks centred at 796 and 973 cm^{-1}. The first peak corresponds to the transverse optic (TO) mode, the second to the longitudinal optic (LO) mode. "The LO band has its intensity dependent on the wavelength of the incident laser". If a 514 nm laser excitation is used, "the LO band had its intensity similar to that of the TO band, but when the 780 nm laser was used, the LO band had intensity much smaller than the TO peak" (Wieligor et al., 2005).

Wieligor and coworker stress the role of the laser power. "Silicon carbide is a material that effectively absorbs light, including the incident laser light. During this process the sample's temperature increases and this may cause frequency shifts. This effect may overlap with shifts due to other effects and must be separated. … To reduce laser induced heating effects, during" their studies, Wieligor and coworkers "applied a very small laser power of 0.01 W, and to collect spectra of high signal to noise ratio" they "used long exposure times." (Wieligor et al., 2005). Moreover, Wieligor and coworkers observe that "with decreasing grain size the intensity of the Raman lines of SiC was decreasing, the LO and TO peaks became increasingly broader and asymmetric, and their frequency shifted". The researchers also remember that Nemanich et al., 1981, "observed *asymmetric broadening of Raman lines* and frequency shifts when the crystal size was decreasing. They explained these effects in terms of the phonon confinement model". Nemanich and coworkers investigated BN microcrystalline samples.

By means of their investigations, Wieligor and coworkers noted that "For small size crystals the TO peak is accompanied by a shoulder on the low frequency side. For SiC of average grain sizes of 400 and 220 nm the shoulder was observed at 765.5 cm^{-1}. For 20 nm crystals it was observed at 761.5 cm^{-1} and for NW-B [sample] at 757 cm^{-1}. … Recently, Rohmfeld et al. showed that the separation between the TO peak and the shoulder reflects the average distance between stacking faults" (Wieligor et al., 2005).

10

Stacking faults are the most common defects observed in silicon carbide (Wieligor and coworkers, mentioning Vetter and Dudley, 2004).

In the article by Wieligor and coworkers, it follows a detailed discussion about Brillouin zone activity in the first-order Raman scattering and about the grain size effect, concluding that, "in view of the discussion of the TO band position dependence on effects other than the crystal size, it is reasonable to assume that the LO band is also affected by the presence of defects, strains and surface layer, and the observed frequency shift cannot be used to evaluate grain sizes. The existence of defects is also manifested by large band widths and the presence of shoulders" (Wieligor et al., 2005).

Let us also report the following observations from Wieligor et al., 2005: "For small particles the number of atoms close to the surface is comparable to that in the interior of the particle. The core-shell model of nanosize crystals assumes that in the core atoms are arranged in the crystallographic structure identical to that of bulk crystal, but the outer layers of the nanocrystals, the shells, although also arranged in the same crystallographic structure, have interatomic distances that are slightly increased (SiC, diamond) or decreased (GaN)" (see references given by Wieligor et al.). "The surface atoms may contribute less to the polarization than the core atoms because of the lack of counter-ions outside the grain" (Wieligor et al., 2005).

Regarding the asymmetry of Raman peak profiles, Gao and Yin, 2017, discuss its origin in the case of Silicon nanocrystals. "The asymmetric peak broadening towards the low-frequency side of the Raman-active mode of Si nanocrystals with the decreasing size has been extensively reported in the literatures". Gao and Yin are proposing an atomic model "to study the origin of the ubiquitous asymmetric peak on the optical phonon fundamental in the Raman spectra of Si nanocrystals". The model "revealed that the observed asymmetric broadening is mainly caused by the surface bond contraction and the quantum confinement". As asserted by Gao and Yin, "The asymmetry and broadening around the main Raman peak in symmetric stretching vibration region undoubtedly correspond to the variant of secondary-structure, which is usually considered as a surface effect of nanocrystals, and assigned as a "surface optical" phonon".

In Gao and Yin we can find the Richter-Wang-Ley (RWL) theory for the Raman intensity, that is the theory which is representing the effect of the phonon confinement in the finite crystal domains, as giving the following intensity: $I(\omega) = \int |C_D(q)|L(\omega, q)dq$. $C_D(q)$ is the Fourier coefficients of an envelope function. D is the nanocrystal size. $L(\omega, q)$ corresponds to the Lorentzian profile "associated to each Raman active phonon" (Gao and Yin). This model is good for microcrystals but not proper for nanocrystals. Gao and Yin, "considered to analyze the Raman spectra of Si nanocrystals by decomposing Si nanocrystal into four type of Si atoms". We find in their model the one-coordinated Si atoms, Si(1), such as the two-, three- and four-coordinated Si atoms, denoted as Si(2), Si(3) and Si (4). Si(1), Si(2) and Si(3) are related to surface atoms, whereas Si(4) is representing the atoms inside the nanocrystallite core. "Each type of Si atoms can produce a Raman subpeak. The Raman spectrum of Si nanocrystals is a sum of four broadened symmetric Lorentzian subpeaks of Si atoms with different coordination. The ratio of the relative integrated intensity between each two different coordinated Si atoms is proportional to their number of atoms".

As we have previously seen, three q-Gaussians components are able, as in the Fig.6, to fit the asymmetric LO mode of SiC (the fit is further improved if four components are used). In the framework of a RWL model, we can assume to use an asymmetric q-Gaussian accompanied by a symmetric q-Gaussian as in the Fig.9. According to the discussion previously given, both approaches can be adopted for fitting asymmetric peaks.

11

References

1. Campbell, I. H., & Fauchet, P. M. (1986). The effects of microcrystal size and shape on the one phonon Raman spectra of crystalline semiconductors. Solid State Communications, 58(10), 739-741.

2. Capitani, G. C., Di Pierro, S., & Tempesta, G. (2007). The 6H-SiC structure model: Further refinement from SCXRD data from a terrestrial moissanite. American Mineralogist, 92(2-3), 403-407.

3. Chafai, M., Jaouhari, A., Torres, A., Antón, R., Martın, E., Jiménez, J., & Mitchel, W. C. (2001). Raman scattering from LO phonon-plasmon coupled modes and Hall-effect in n-type silicon carbide 4H–SiC. Journal of Applied Physics, 90(10), 5211-5215.

4. Ciuryło, R., Domysławska, J., & Trawiński, R. S. (1993). Differential equation for asymmetric Voigt profile. Acta Physica Polonica A, 83(4), 425-430.

5. Devi, S. (2021). Asymmetric Tsallis distributions for modeling financial market dynamics. Physica A: Statistical Mechanics and Its Applications, 578, 126109.

6. El Mendili, Y., Vaitkus, A., Merkys, A., Gražulis, S., Chateigner, D., Mathevet, F., Gascoin, S., Petit, S., Bardeau, J.-F., Zanatta, M., Secchi, M., Mariotto, G., Kumar, A., Cassetta, M., Lutterotti, L., Borovin, E., Orberger, B., Simon, P., Hehlen, B., & Le Guen, M. (2019). Raman Open Database: first interconnected Raman–X-ray diffraction open-access resource for material identification. Journal of Applied Crystallography, 52(3), 618-625. doi: 10.1107/s1600576719004229

7. Gao, Y., & Yin, P. (2017). Origin of asymmetric broadening of Raman peak profiles in Si nanocrystals. Scientific Reports, 7(1), 43602.

8. Hanel, R., Thurner, S., & Tsallis, C. (2009). Limit distributions of scale-invariant probabilistic models of correlated random variables with the q-Gaussian as an explicit example. The European Physical Journal B, 72(2), 263.

9. Hasdeo, E. H., Nugraha, A. R., Dresselhaus, M. S., & Saito, R. (2014). Breit-Wigner-Fano line shapes in Raman spectra of graphene. Physical Review B, 90(24), 245140.

10. Kiefert, L., Hänni, H. A., & Schmetzer, K. (2002). Russian synthetic moissanite. Acta Universitatis Carolinae: Geologica, 46(1), 40-41.

11. Kirillov, S. A. (2004a). Novel approaches in spectroscopy of interparticle interactions. Raman line profiles and dynamics in liquids and glasses. Journal of molecular liquids, 110(1-3), 99-103.

12. Kirillov, S. (2004b). Novel approaches in spectroscopy of interparticle interactions. Vibrational line profiles and anomalous non-coincidence effects. In Novel Approaches to the Structure and Dynamics of Liquids: Experiments, Theories and Simulations; Springer: Berlin/Heidelberg, Germany, 2004; pp. 193–227

13. Koyanagi, T., Lance, M. J., & Katoh, Y. (2016). Quantification of irradiation defects in beta-silicon carbide using Raman spectroscopy. Scripta Materialia, 125, 58-62.

14. Liu, L. Z., Wang, J., Wu, X. L., Li, T. H., & Chu, P. K. (2010). Longitudinal optical phonon–plasmon coupling in luminescent 3C–SiC nanocrystal films. Optics letters, 35(23), 4024-4026.

15. Meier, R. J. (2005). On art and science in curve-fitting vibrational spectra. Vibrational spectroscopy, 2(39), 266-269.

16. Naudts, J. (2009). The q-exponential family in statistical physics. Central European Journal of Physics, 7, 405-413.

17. Nemanich, R. J., Solin, S. A., & Martin, R. M. (1981). Light scattering study of boron nitride microcrystals. Physical Review B, 23(12), 6348.

18. Prawer, S., & Nemanich, R. J. (2004). Raman spectroscopy of diamond and doped diamond. Philosophical Transactions of the Royal Society of London. Series A: Mathematical, Physical and Engineering Sciences, 362(1824), 2537-2565.

19. Rashid, M., Horrocks, B. R., Healy, N., Goss, J. P., & Horsfall, A. B. (2016). Optical properties of mesoporous 4H-SiC prepared by anodic electrochemical etching. Journal of Applied Physics, 120(19).

20. Richter, H., Wang, Z. P., & Ley, L. (1981). The one phonon Raman spectrum in microcrystalline silicon. Solid State Communications, 39(5), 625-629.

21. Rohmfeld, S., Hundhausen, M., & Ley, L. (1998). Raman scattering in polycrystalline 3 C− SiC: Influence of stacking faults. Physical Review B, 58(15), 9858.

22. Schmid, M., Steinrück, H. P., & Gottfried, J. M. (2014). A new asymmetric Pseudo-Voigt function for more efficient fitting of XPS lines. Surface and Interface Analysis, 46(8), 505-511.

23. Shiryaev, A. A., Griffin, W. L., & Stoyanov, E. (2011). Moissanite (SiC) from kimberlites: Polytypes, trace elements, inclusions and speculations on origin. Lithos, 122(3-4), 152-164.

24. Sparavigna, A. (2002). Lattice thermal conductivity in cubic silicon carbide. Physical Review B, 66(17), 174301.

25. Sparavigna, A. C. (2022). Entropies and Logarithms. Zenodo. DOI 10.5281/zenodo.7007520

26. Sparavigna, A. C. (2023). q-Gaussian Tsallis Line Shapes and Raman Spectral Bands. International Journal of Sciences, 12(03), 27-40. http://dx.doi.org/10.18483/ijSci.2671

27. Sparavigna, A. C. (2023). q-Gaussian Tsallis Functions and Egelstaff-Schofield Spectral Line Shapes. International Journal of Sciences, 12(03), 47-50. http://dx.doi.org/10.18483/ijSci.2673

28. Sparavigna, A. C. (2023). q-Gaussian Tsallis Line Shapes for Raman Spectroscopy (June 7, 2023). SSRN Electronic Journal. http://dx.doi.org/10.2139/ssrn.4445044

29. Sparavigna, A. C. (2023). Formamide Raman Spectrum and q-Gaussian Tsallis Lines (June 12, 2023). SSRN Electronic Journal. http://dx.doi.org/10.2139/ssrn.4451881

30. Sparavigna, A. C. (2023). Tsallis and Kaniadakis Gaussian functions, applied to the analysis of Diamond Raman spectrum, and compared with Pseudo-Voigt functions. Zenodo. https://doi.org/10.5281/zenodo.8087464

31. Sparavigna A. C. (2023). Tsallis q-Gaussian function as fitting lineshape for Graphite Raman bands. ChemRxiv. Cambridge: Cambridge Open Engage; 2023.

32. Sparavigna A. C. (2003). Fitting q-Gaussians onto Anatase TiO2 Raman Bands. ChemRxiv. Cambridge: Cambridge Open Engage; 2023.

33. Sparavigna, A. (2023). Q-Gaussians and the SERS Spectral Bands of L-Cysteine and Cysteamine. ChemRxiv. doi:10.26434/chemrxiv-2023-9swp9-v2

34. Sun, H. Y., Lien, S. C., Qiu, Z. R., Wang, H. C., Mei, T., Liu, C. W., & Feng, Z. C. (2013). Temperature dependence of Raman scattering in bulk 4H-SiC with different carrier concentration. Optics Express, 21(22), 26475-26482.

35. Tsallis, C. (1988). Possible generalization of Boltzmann-Gibbs statistics. Journal of statistical physics, 52, 479-487.

36. Tsallis, C. (1995). Some comments on Boltzmann-Gibbs statistical mechanics. Chaos, Solitons & Fractals, 6, 539-559.

37. Umarov, S., Tsallis, C., Steinberg, S. (2008). On a q-Central Limit Theorem Consistent with Nonextensive Statistical Mechanics. Milan J. Math. Birkhauser Verlag. 76: 307–328. doi:10.1007/s00032-008-0087-y. S2CID 55967725.

38. Vetter, W. M., & Dudley, M. (2004). Characterization of defects in 3C-silicon carbide crystals. Journal of crystal growth, 260(1-2), 201-208.

39. Wieligor, M., Wang, Y., & Zerda, T. W. (2005). Raman spectra of silicon carbide small particles and nanowires. Journal of Physics: Condensed Matter, 17(15), 2387.

40. Xu, S., Wu, W., Xiao, W., Yang, J., Chen, J., Ji, S., & Liu, Y. (2008). Moissanite in serpentinite from the Dabie Mountains in China. Mineralogical Magazine, 72(4), 899-908.